Long-Range Order in Laser-Cooled, Atomic-Ion Wigner Crystals Observed by Bragg Scattering

Joseph N. Tan, J. J. Bollinger, B. Jelenkovic,* and D. J. Wineland

Time and Frequency Division, National Institute of Standards and Technology, Boulder, Colorado 80303

(Received 26 June 1995)

We report the first observation of Bragg scattering from atomic ions confined in an electromagnetic trap. The results reveal long-range order and give evidence for bulk behavior in a strongly coupled collection of laser-cooled $^9Be^+$ ions in a Penning trap. Long-range order emerges in approximately spherical clouds with as few as 5×10^4 ions (cloud radius $r_0 \approx 37a$ where $a \equiv$ Wigner-Seitz radius). Bulk behavior is evident with 2.7×10^5 trapped ions ($r_0 \approx 65a$), with Bragg scattering patterns characteristic of a body-centered cubic lattice.

Systems of crystallized charged particles have gained wide interest, with implications for the pure Coulomb systems of one-component plasmas [1], trapped atomic ions [1–3], ion storage rings [4], and dense astrophysical matter [5], and for the shielded Coulomb systems of colloidal suspensions [6] and dusty plasmas [7]. For example, Paul rf traps have been used to study crystallization and melting of small "Coulomb clusters" [8]. In both the rf and Penning traps, cold ions form shell structures when the dimensions of the system exceed a few interparticle spacings [9,10]. Such transitions of Coulomb fluids into crystal-like structures are examples of Wigner crystallization in the classical regime (i.e., the wave functions of the particles do not overlap). However, the pure Coulomb systems realized so far are not large enough to neglect surface effects and hence do not allow observation of infinite-volume or bulk behavior [11]. For example, the "micromotion" of ions in the rf trap, which generates the trapping potential, can cause heating which limits the smallest dimension of laser-cooled ion collections to a few interparticle spacings [3]. The drawback of the Penning trap (which uses static trapping fields) *vis-à-vis* the rf trap is that the ions rotate about the trap magnetic field—this has hindered imaging of the ion crystals as seen in Paul traps [3,8,10]. However, the Penning trap, which has no micromotion heating, can potentially store very large systems of laser-cooled ions and hence was used in the studies here.

In related works, optical lattices formed by the interference of intersecting laser beams have been used to localize and cool neutral atoms [12,13]. Unlike the ion Wigner crystals, optical lattices are not formed by the interaction of the confined atoms; rather, they conform to the periodic confinement wells created by the laser standing waves. Also, trapped ions differ from systems of colloidal suspensions and dusty plasmas in that the ions interact through a pure Coulomb (rather than a Yukawa-type) potential, and the charges (q) and masses (m) of the particles are identical.

A system of ions confined in a Penning trap (hereafter called an "ion cloud") is an example of a one-component plasma (OCP) [1]. A OCP is a system of identical charged particles that is neutralized by a uniform-density background of opposite charge. The thermodynamic properties of an ion OCP are fully characterized by the coupling parameter

$$\Gamma \equiv \frac{1}{4\pi\epsilon_0} \frac{q^2}{ak_BT} , \qquad (1)$$

the ratio of the nearest-neighbor Coulomb interaction energy to the thermal energy (k_BT) of an ion. The Wigner-Seitz radius a, a measure of the interparticle spacing, is defined by $4\pi a^3 n_0/3 = 1$, where n_0 is the density of the neutralizing background (which is formally equivalent to the confinement fields in ion traps), and is equal to the ion density at low temperatures [1]. An unbounded OCP is predicted to exhibit liquidlike behavior for $\Gamma > 2$ and undergo a liquid-solid phase transition to a bcc lattice at $\Gamma = 172$ [14]. The OCP has become one of the most carefully studied models in statistical physics because the interaction is simple and because of its importance in understanding dense astrophysical plasmas [5]. In contrast to the growing number of theoretical works, there are few laboratory systems to test the models. Until now, only shell structures have been observed with $N < 1.5 \times 10^4$ ions in a Penning trap [9], and in a race-track rf trap [3,10]. This shell phase can be viewed as arising from the strong influence of the curved surface of a small cloud [11]. Simulation studies show that the ions in each shell form distorted (2D) hexagonal lattices, exhibiting short-range order with little correlation between shells [4,15].

We report here the first observation of Bragg scattering from laser-cooled ions in a trap [16]. In ion clouds with all dimensions much larger than the Wigner-Seitz radius, we find interesting departures from the earlier observed shell phase [9]. Shell structures are still observed with $N < 2 \times 10^4$ ions (or radii $r_0 < 27a$ for spherical clouds). Long-range order emerges with as few as $N \approx 5 \times 10^4$ ions ($r_0 \approx 37a$). We show that for $N \approx 2.7 \times 10^5$ ions ($r_0 \approx 65a$) the Bragg scattering pat-

tern is consistent with a bcc lattice. The ion crystals are estimated to be >150 μm ($\sim 20a$) long on a side.

Theoretical estimates indicate that $r_0 \gtrsim 50a$ is required for bulk behavior [11,17]. We have built a large Penning trap wherein clouds with $N \leq 2.7 \times 10^5$ ions ($r_0 \leq 65a$) and Γ values as high as 600 have been attained. The trap is formed by a 127 mm long stack of cylindrical electrodes with 40.6 mm inner diameter, in a 10^{-8} Pa vacuum. A NMR superconductive magnet provides a uniform magnetic field ($B_0 = 4.5$ T) parallel to the trap axis (z axis), confining the ions in orbits around this axis (cyclotron frequency of $\Omega/2\pi = qB_0/m = 7.55$ MHz). A static electric field, generated by applying $V_0 = 1$ kV between the end and central electrodes, confines the ions along the z axis near the center ($z = 0$) of the trap (a single ion oscillates at $\omega_z/2\pi = 795$ kHz).

The trapped ^{9}Be$^+$ ions are cooled by a laser beam propagating along the z axis (Fig. 1) and are optically pumped into the $2s\,^2S_{1/2}(M_I = -\frac{3}{2}, M_J = -\frac{1}{2})$ state by tuning the laser frequency ($\lambda \approx 313$ nm) slightly below the $2s\,^2S_{1/2}(-\frac{3}{2}, \frac{1}{2}) \rightarrow 2p\,^2P_{3/2}(-\frac{3}{2}, -\frac{3}{2})$ resonance frequency [2]. A laser-cooled ion cloud first condenses into a bounded fluid state (a liquid drop). In a Penning trap with quadratic potential and negligible image charge effects, a laser-cooled ion cloud forms a uniform density spheroid bounded by $(x^2 + y^2)/r_s^2 + z^2/z_s^2 = 1$ (for a spherical cloud, $r_s = z_s \equiv r_0$) [18]. The residual thermal motions are superimposed upon a rigid rotation of the ion cloud about the z axis. The aspect ratio $\alpha \equiv z_s/r_s$ of the spheroid varies with its rigid rotation frequency ω_r [18,19]. A laser beam directed normal to the z axis (not shown in Fig. 1 and turned off during the Bragg scattering) can exert a torque and change ω_r within 40.8 kHz $< \omega_r/2\pi < 7.51$ MHz, thus controlling the shape and density of the cloud [18]. An $f/5$ imaging system along the
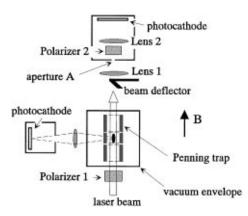

FIG. 1. Schematic diagram (not to scale) for detection of Bragg scattering from an ion cloud, shown as a small prolate spheroid, inside a Penning trap. An $f/5$ imaging system (left) monitors the shape of the cloud, thereby giving the ion density. The diffraction pattern is relayed to the upper photocathode, filtered by a small aperture (A) and crossed polarizers, as described in the text.

x axis, with a laser beam along the z axis (beam waist ~ 0.4 mm $\gtrsim r_s$, power ~ 200 μW), gives a side-view image of the ion cloud, thus monitoring z_s and r_s which, in turn, yields α, a, ω_r, n_0, and N [18].

Bragg scattering is used to study the spatial correlations because the rigid rotation of the ion cloud makes it difficult to image a crystal lattice. The photons resonantly scattered by the ions interfere to form Bragg-scattering peaks at certain angles determined by the crystal lattice. Because $\lambda/a \sim 0.04$, the diffraction pattern occurs very close to the laser beam direction (Fig. 1), within about 0.1 rad. Since the ions scatter far fewer photons than the vacuum windows, special care is needed to minimize this potentially strong background.

As shown in Fig. 1 (not to scale), the laser beam ($\mathbf{k}_i = 2\pi\hat{\mathbf{z}}/\lambda$) propagates first through a linear polarizer 1, and then into the vacuum chamber. Upon exiting the ion trap, the laser beam is diverted away from the detector by a set of mirrors. The photons scattered by the ions ($\mathbf{k}_s = 2\pi\hat{\mathbf{k}}_s/\lambda$) are collected by lens 1 ($f = 19$ cm, $z = 25.5$ cm from the ions), forming an image of the ion cloud at a small aperture (A) to reduce the background. The diffraction pattern is then relayed by lens 2 ($f \approx 24$ cm) to the photocathode of a photon-counting imager ($z \approx 160$ cm). The linear polarizer 2 is inserted after the aperture. The polarization axes of polarizers 1 and 2 are crossed to attenuate, with extinction ratio $\geq 6 \times 10^5$, the stray light that leaks through the small aperture and has the same polarization as polarizer 1. The photons scattered from the ions, however, are attenuated only by a factor of 2 since they are mainly circularly polarized.

The Bragg scattering from ion clouds with $N \gtrsim 5 \times 10^4$ ions ($r_0 \gtrsim 37a$) exhibits long-range order characteristic of a crystal. Because of the ion cloud rotation ($\omega_r/2\pi \sim 10^5$ Hz), the dots in a crystalline Laue pattern are rotated into rings. (A ring pattern will also be produced by a crystalline powder or fluid.) Figure 2(a) gives an example of a Bragg scattering pattern obtained with $N = 2.7 \times 10^5$ trapped ions with long-range order. The circular intensity maxima are Bragg peaks, with radii inversely proportional to the Wigner-Seitz radius a. To facilitate analysis, a differential scattering cross section is generated from each diffraction pattern by averaging the photon counts azimuthally about the z axis, as illustrated in Fig. 2(b). A density-independent plot is obtained by using the dimensionless parameter Δka, where Δk is the length of the vector $\boldsymbol{\Delta k} = \mathbf{k}_i - \mathbf{k}_s$. This can be compared with the interference function [20] or the static structure factor $S(\Delta ka)$ calculated for various systems. For incoherent scattering, $S(\Delta ka) = 1$. The short correlation lengths ($\sim a$) of the fluid and shell phases are reflected in their $S(\Delta ka)$, shown in Fig. 2(c) [21], which have only one strong, narrow peak. In contrast, Fig. 2(b) has four strong, narrow peaks indicating the presence of a crystal. Similar diffraction patterns for
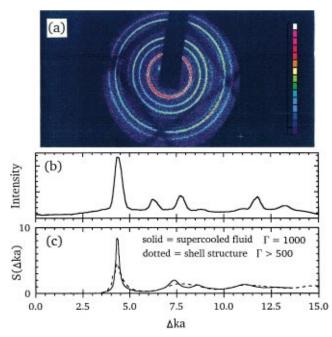
FIG. 2(color). Observed Bragg scattering from $N = 2.7 \times 10^5$ ions (a) and (b) compared with the $S(\Delta ka)$ calculated for a supercooled fluid and an $N = 5 \times 10^3$ ion cloud with shells (c) [21]. The diffraction pattern ions (a) is partially blocked, as indicated by a rectangular shadow due to the laser beam deflector and a square shadow due to a wire mech. The color scale is logarithmic. The total flux reaching the detector is $\simeq 1 \times 10^8$ photons/s but is attenuated to avoid saturating the photocathode. The field of view subtends a 5.4° scattering angle from the z axis. The differential cross section (b) is obtained by azimuthally averaging (a) about the z axis.

$N > 5 \times 10^4$ ions ($r_0 > 37a$) have been obtained with up to nine narrow Bragg peaks. Such long-range order is not observed every time we cooled an ion cloud. In this case, if a crystal was formed, the reason it was not observed may be that some crystal orientations did not produce Bragg peaks.

The crystal structure may be determined from the positions of the Bragg peaks [22]. For an unbounded OCP the minimum-energy structure is a body-centered cubic (bcc) lattice [14]. However, there are metastable structures with slightly higher energies, such as the face-centered cubic (fcc) and the hexagonal close-packed (hcp) lattices [11,23]. In a bounded ion cloud, residual surface effects may determine which structure dominates. An analysis of data from a cloud with $N \gtrsim 2.7 \times 10^5$ ions ($r_0 \approx 65a$) shows that the diffraction patterns are consistent with a bcc lattice. Figure 3(a), the evidence of bulk behavior, shows a histogram of the number of observed Bragg peaks (not intensity) as a function of Δka, constructed with no adjustable parameters from 14 diffraction patterns obtained from the same ion cloud ($N = 2.7 \times 10^5$ ions) with various Wigner-Seitz radii ($20 < a/\lambda < 27$). Typically the ion cloud was heated and recooled several times between each recorded pattern.
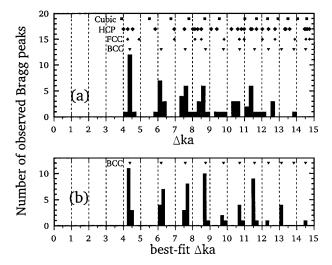

FIG. 3. Evidence of bulk behavior in an ion OCP. Histogram (a) counts the number of observed peaks (not intensity) from various diffraction patterns of the same cloud ($N = 2.7 \times 10^5$ ions), with no adjustable parameters (a is determined from the observed α). By fitting to the bcc lattice for the Wigner-Seitz radius a, even the high Δka peaks are observed to be consistent with a bcc lattice (b). The ticks indicate the location of Bragg peaks for various lattice types.

The scatter of the peak positions in Fig. 3(a) is consistent with the $\sim 5\%$ uncertainty in the determination of the Wigner-Seitz radius a from the observed value of the aspect ratio α. This uncertainty also makes comparison with known lattices difficult for $\Delta ka > 10$, where the density of Bragg peaks is higher. However, for $\Delta ka < 10$, the bcc lattice is the best match to the observed patterns. Having identified the lattice, we can also determine the Wigner-Seitz radius a by fitting each pattern to the calculated bcc peaks. With these fitted values of a, the histogram Fig. 3(b) matches the bcc lattice very well even as far as $\Delta ka \sim 14$.

The minimum size of the ion crystals can be estimated from the intensity widths of the Bragg peaks [see Fig. 2(b)]. For a perfect crystal of characteristic length L, the finite-size broadening of the Bragg peaks is estimated by the formula $L \approx \lambda / \Delta$, where Δ is the angular FWHM of the Bragg peak [24]. We find that, on average, $\Delta \sim 2$ mrad. This gives $L \sim 150$ μm ($\sim 20a$). With the typical density ($n_0 \sim 5 \times 10^8/\mathrm{cm}^3$), this corresponds to a few thousand ions per crystal. This is a lower limit since the observed widths can be instrumentally broadened, as suggested by the small change in Δ with N.

The relative intensity of the Bragg peaks indicates that the ions do not freeze into a "powdered" sample of randomly oriented crystals. For example, in some cases, peaks expected in such a powder pattern are missing. The crystallized region may be surrounded by at least $\simeq 20$ shells on the cloud surface (based on a simulation with 2×10^4 ions) [25]. For a cloud with 2.7×10^5 ions these boundary shells contain about 2.3×10^5 ions.

The scattering from the shells may contribute to the size of the first Bragg peaks, but will produce a fairly flat background [$S(\Delta ka) \sim 1$] for the other peaks. As shown in Fig. 2(b), the Bragg peaks are superimposed upon a broad background. Many of the observed Bragg peaks are often as large as, if not a few times larger than, the background. If these are Bragg peaks from a single crystal, the crystal must contain $N \sim 10^4$ ions (for $L \sim 240$ μm or $35a$ on a side) in order to produce peak intensities greater than the background due to 2.3×10^5 ions.

In the future, we hope to remove the averaging due to the rigid rotation by stroboscopic detection of the Bragg scattering. This could be useful in determining whether the ions form more than one crystal. It may reveal other types of crystals in the ion OCP. Quasicrystals, for example, would produce a fivefold azimuthal symmetry in the diffraction pattern [26]. The uncertainty in Wigner-Seitz radius a can be reduced by measuring ω_r directly [18].

---

   *On leave from the Institute of Physics, University of Belgrade, Yugoslavia.

 [1] J. H. Malmberg and T. M. O'Neil, Phys. Rev. Lett. **39**, 1333 (1977).
 [2] J. J. Bollinger and D. J. Wineland, Phys. Rev. Lett. **53**, 348 (1993).
 [3] H. Walther, Adv. At. Opt. Phys. **31**, 137 (1993).
 [4] A. Rahman and J. P. Schiffer, Phys. Rev. Lett. **57**, 1133 (1986); J. P. Schiffer, Phys. Rev. Lett. **61**, 1843 (1988); D. Habs, Max-Planck Institut fur Kernphysik, Heidelberg, Report No. MPI H-1987-V10, 1987 (unpublished).
 [5] S. Ogata and S, Ichimaru, Astrophys. J. **361**, 511 (1990); T. Strohmayer et al., Astrophys. J. **375**, 679 (1991).
 [6] N. A. Clark, A. J. Hurd, and B. J. Ackerson, Nature (London) **281**, 57 (1979); C. A. Murray, W. O. Sprenger, and R. A. Weak, Phys. Rev. B **42**, 688 (1990); L. B. Chen et al., Phys. Rev. Lett. **69**, 688 (1992).

 [7] J. H. Chu and Lin I, Phys. Rev. Lett. **72**, 4009 (1994); H. Thomas, G. E. Morfill, V. Demmel, and J. Goree, Phys. Rev. Lett. **73**, 652 (1994).
 [8] R. F. Wuerker et al., J. Appl. Phys. **30**, 342 (1959); F. Diedrich et al., Phys. Rev. Lett. **59**, 2931 (1987); D. J. Wineland et al., Phys. Rev. Lett. **59**, 2935 (1987).
 [9] S. L. Gilbert, J. J. Bollinger, and D. J. Wineland, Phys. Rev. Lett. **60**, 2022 (1988).
[10] G. Birkl, S. Kassner, and H. Walther, Nature (London) **357**, 310 (1992).
[11] D. H. E. Dubin, Phys. Rev. A **40**, 1140 (1989).
[12] P. Verkerk et al., Phys. Rev. Lett. **68**, 3861 (1992); P. S. Jessen et al., Phys. Rev. Lett. **69**, 49 (1992); A. Hemmerich and T. W. Hansch, Phys. Rev. Lett. **70**, 410 (1993).
[13] D. R. Meacher et al., Phys. Rev. Lett. **74**, 1958 (1995), and references therein.
[14] W. L. Slattery, G. D. Doolen, and H. E. DeWitt, Phys. Rev. A **26**, 2255 (1982); D. H. E. Dubin, Phys. Rev. A **42**, 4972 (1990).
[15] D. H. E. Dubin and T. M. O'Neil, Phys. Rev. Lett. **60**, 511 (1988); R. W. Hasse and J. P. Schiffer, Ann. Phys. (N.Y.) **203**, 419 (1990).
[16] Some preliminary results are in J. N. Tan et al., Non-neutral Plasma Physics II, edited by J. Fajans and D. H. E. Dubin (AIP Press, New York, 1995), p. 215.
[17] R. W. Hasse and V. V. Avilov, Phys. Rev. A **44**, 4506 (1991).
[18] J. J. Bollinger et al., Phys. Rev. A **54**, 525 (1993).
[19] L. R. Brewer et al., Phys. Rev. A **38**, 859 (1988).
[20] A. Guinier, X-Ray Diffraction in Crystals, Imperfect Crystals, and Amorphous Bodies (Dover Publications, Inc., New York, 1994), p. 29.
[21] The supercooled fluid $S(\Delta ka)$, calculated for an unbounded system with $\Gamma = 1000$, is from Fig. 6(b) in S. Ichimaru et al., Phys. Rep. **149**, 91 (1987). The shell phase $S(\Delta ka)$ is calculated from simulation data for an $N = 5000$ spherical cloud and $\Gamma > 500$, received from J. P. Schiffer. Similar shells $S(\Delta ka)$ have been calculated by D. H. E. Dubin.
[22] N. W. Ashcroft and N. D. Mermin, Solid State Physics (Holt, Reinhart, and Winston, Philadelphia, 1976), pp. 104–107.
[23] S. Ogata, Phys. Rev. A **45**, 1122 (1992).
[24] Guinier (Ref. [20]), pp. 125–130.
[25] J. P. Schiffer, in Non-neutral Plasma II, edited by J. Fajans and D. H. E. Dubin (AIP, New York, 1995), p. 191.
[26] M. V. Jaric, Phys. Rev. B **34**, 4685 (1986); S. Ogata and S. Ichimaru, Phys. Rev. A **39**, 1333 (1989); H. C. Jeong and P. J. Steinhardt, Phys. Rev. Lett. **73**, 1943 (1994).